2011 American Control Conference
on O'Farrell Street, San Francisco, CA, USA
June 29 - July 01, 2011

Actuator Sizing of a Quadruple Pendulum for Advanced Gravitational Wave Detectors

Brett Shapiro, Nergis Mavalvala, Kamal Youcef-Toumi

***Abstract*— The Laser Interferometer Gravitational-Wave Observatory (LIGO) has begun a major set of upgrades to reach a sensitivity better than $10^{-19}\,\mathrm{m}/\sqrt{\mathrm{Hz}}$ in the $10\,\mathrm{Hz}$ to $10\,\mathrm{kHz}$ frequency band. This advance is expected to bring gravitational wave observations of relativistic astrophysical events such as black hole mergers and supernovae into the realm of regular astronomy. These upgrades require complex vibration isolation systems to better decouple the test masses from ground disturbances. These high performance systems require correspondingly more complex and aggressive active control loops to meet the increased demand in instrument sensitivity. Appropriately sized actuators are essential to achieving the necessary control performance while limiting the cost, noise, and complexity associated with larger actuators. This paper applies the plant's pseudoinverse transfer function to analyze the least squares dynamic range required by the actuators to reject the stochastic disturbances exciting the Advanced LIGO quadruple pendulum isolation systems.**

I. Introduction

Gravitational waves (GWs), predicted to exist by Einstein's General Theory of Relativity, are distortions of spacetime that, due to their weak interactions, until now have not been directly detected. Over the next several years, the Laser Interferometer Gravitational-Wave Observatory (LIGO) [1], [2] and other highly sensitive observatories will undergo upgrades that should make detections of GWs possible [3].

The upgrade of LIGO, known as Advanced LIGO [4], aims to push the spectral displacement sensitivity of the detectors down to measure GWs between $10\,\mathrm{Hz}$ and $10\,\mathrm{kHz}$. These measurements require a sensitivity better than $10^{-19}\,\mathrm{m}/\sqrt{\mathrm{Hz}}$ in this band. The low frequency end of this sensitivity spectrum is dominated by natural seismic disturbances. Multiple cascaded seismic isolation systems are employed to reach this exquisite sensitivity at these low frequencies.

The final stage of the most sensitive of these isolation systems is a quadruple pendulum, which directly suspends the interferometer mirrors [5]. Active control loops position these mirrors by pushing on the various stages of the quadruple pendulum ("quad").

The actuators employed by these controls loops are critical to LIGO's performance. Undersized actuators will not generate sufficient force to adequately position the mirrors. Oversized actuators risk poor noise performance, cost, and overall complexity.

Brett Shapiro (bshapiro@mit.edu) and Nergis Mavalvala (nergis@ligo.mit.edu) are with the LIGO Laboratory at the Massachusetts Institute of Technology in Cambridge, MA 02139, USA

Kamal Youcef-Toumi (youcef@MIT.EDU) is with the Department of Mechanical Engineering at the Massachusetts Institute of Technology

For linear SISO systems it is relatively easy to estimate the force needed by an actuator by either designing a simple controller or inverting the plant to estimate the required force from the desired trajectory. For MIMO systems this analysis becomes more complex and less obvious, especially when there are more inputs than outputs.

This paper applies the pseudoinverse of the pendulum's rectangular transfer function matrix to determine the least mean square actuation required by the quadruple pendulum isolation systems to reject the anticipated stochastic disturbance spectrum. This analysis is used to validate the current actuator design by taking into account the actuator responses, actuator dynamic ranges, and the pendulum response. The power of this method is that it sets a minimum actuation requirement without any feedback loop design. The analysis also provides hints as to how the most effective control loops might be designed by quantifying the relative effectiveness of each actuator as a function of frequency.

II. The LIGO Interferometer

Fig. 1 below is a simplified schematic diagram of the LIGO optical system. Fig. 2 is an aerial photograph of the observatory in Hanford, WA.

The LIGO detectors comprise power-recycled Michelson interferometers with $4\,\mathrm{km}$ long Fabry-Perot cavities in each arm. A laser injects $1064\,\mathrm{nm}$ (infrared) light into the beam splitter that splits the light equally into the two orthogonal arms. The Fabry-Perot cavities in each arm of the Michelson, comprising an input test mass (ITM) and an end test mass (ETM), store the laser light to increase the phase sensitivity of the interferometer. The light will make approximately 100

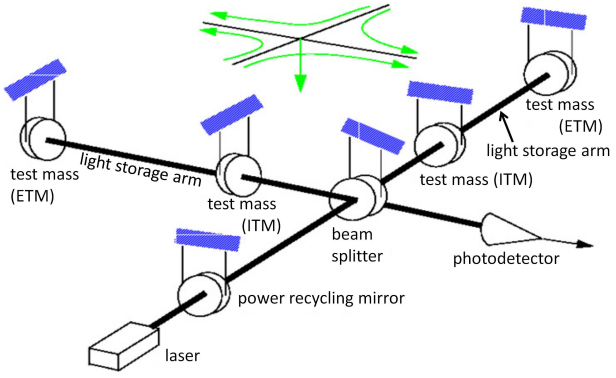

Fig. 1. A simplified schematic diagram of a LIGO Observatory (not to scale) . The propagating GW, indicated by the arrow pointing down towards the interferometer from above, alters the differential length of the two 4 km perpendicular light storage arms. This differential length is measured with the amplitude of the light on the photodetector [3].

Fig. 2. The LIGO Hanford Observatory in Washington State [4].

round trips between these optics. The ETMs and ITM are the most sensitive optics because of the multiple reflections. These are the mirrors suspended from quadruple pendulums.

The light returning from each arm cavity recombines at the beam splitter, and is detected on a photodetector at the antisymmetric (output) port of the beam splitter. Measuring the intensity of the light at this photodetector provides a measure of the phase difference of the light in each arm, and thus the differential length. The differential length is linearly proportional to the amplitude of the GW passing through the detector [3].

In order to measure the weakly interacting GWs from expected astrophysical sources such as coalescing binary neutron stars or black holes [6], the interferometer has to achieve the extremely small sensitivity requirement mentioned in Section I. Fig. 3 shows a plot of the Advanced LIGO sensitivity goal and the various noise and disturbance sources that contribute to it. The optics are suspended as pendulums to decouple them from ground motion (the black seismic 'cutoff' line) above $10\,\mathrm{Hz}$. The pendulums are themselves isolated by a series of pre-isolation stages.

The 'Advanced LIGO Total Noise' curve shown in Fig. 3 represents not only the expected sensitivity to GWs, but the open loop error signal between the differential length of the two arms. To maintain the interferometer at its optimal operating point the active mirror positioning control loops must reduce this signal to a tolerance of $10^{-15}\mathrm{m_{RMS}}$ [7]. Most of this suppression is required below 1 Hz (not shown) where this open loop error levels off above $10^{-7}\mathrm{m}/\sqrt{\mathrm{Hz}}$. This control is applied by pushing on the two ETMs in equal and opposite directions.

III. Quadruple Pendulum Design

The quadruple pendulum is used to suspend the ETM and ITM optics, the most sensitive in the instrument. Fig. 4 provides an illustration of the pendulum and Fig. 5 a photograph of a prototype. It is a stable pendulum consisting of two hanging vertical chains of four masses each. The masses on each chain are numbered top down 1 through 4, where the fourth mass on the main (front) chain is a highly reflective interferometer mirror. In each chain the top two masses are approximately $22\,\mathrm{kg}$ and the lower two masses $40\,\mathrm{kg}$. The main and reaction chains are about $2\,\mathrm{m}$ from top to bottom and hang $5\,\mathrm{mm}$ apart. Each mass of the pendulum is modeled as a rigid body connected elastically by very lightly damped springs to the neighboring masses. Consequently, a second order differential equation is associated with each mass providing f^{-2} isolation above the pendulum's resonant frequencies, where f represents frequency. Thus, by using four masses a performance of f^{-8} is achieved. In this way the pendulum realizes six to seven orders of magnitude of seismic isolation in the single decade between its mechanical resonances and the low frequency end ($10\,\mathrm{Hz}$) of LIGO's sensitivity requirement. The reaction (back) chain is used to provide a quiet actuation platform to filter any disturbance or noise that might couple through the actuators.

There are six collocated sensor/actuator devices called OSEMs (Optical Sensor Electro-Magnet) placed around each top mass and referenced to the ground. These are used to damp the mechanical resonances of the pendulum and provide low frequency mirror positioning control. Fig. 6 includes an illustration of this device. The mechanical resonances, generally between $0.5\,\mathrm{Hz}$ and $5\,\mathrm{Hz}$, are purposely designed with very high quality factors to optimize the spectrum of thermally excited stochastic motions of the mirror. Damping control is permitted only at the top mass since the OSEM sensor noise is non-negligible compared to the high sensitivity required. As a result, the pendulum mechanically attenuates the sensor noise through the pendulum chain below. All modes of vibration are designed to couple to the top mass to ensure controllability for the damping loops [5].

The position and angular control of the mirror, in addition to low frequency control with the top mass actuators, is done with actuators placed between the main and reaction chains at the second, third, and fourth masses down. The pendulum is designed to split the mirror control between the various stages so that larger and noisier low frequency control forces are applied to the higher masses where there is better mechanical attenuation to the mirror. The second and third masses have four OSEMs each, and at the bottom mass there are four electrostatic actuators known as the Electrostatic Drive (ESD). The error signal sent to each of these stages is the position of only the bottom mass measured directly from interferometric signals. The OSEM sensors here are used only for the mechanical assembly of the quad.

IV. Actuator Specifications

A. Optical Sensor Electro Magnet (OSEM)

The OSEMs at the pendulum's top mass provide sensing and actuation for active damping control of the mechanical resonances. They are also used for low frequency control of the mirror. A detailed description is found in [8].

These OSEM actuators contain an $8\,\mathrm{mm}$ long, 800 turn coil of wire that actuates on $10\,\mathrm{mm}$ long by $10\,\mathrm{mm}$ diameter NdBFe, nickel plated magnets attached to the top mass. This coil-magnet pair produces $2.05\,\mathrm{N/A}$. The coil current is driven by a current driver which includes a filter to reduce

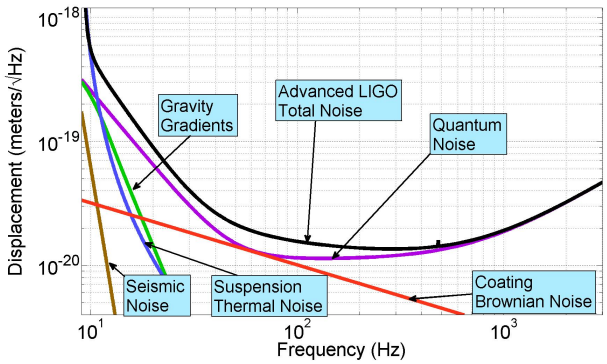

Fig. 3. Projected displacement spectral density limit for the Advanced LIGO design and the contributing noise sources. Adapted from [4].

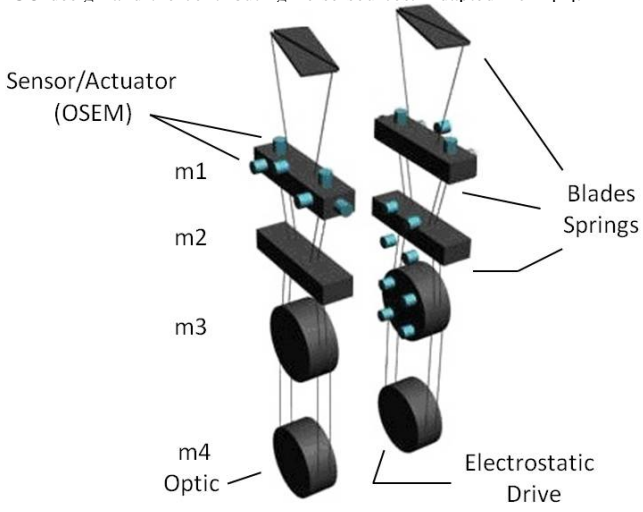

Fig. 4. Illustration of the quadruple pendulum. It consists of two chains, a main chain and a reaction chain. The bottom mass of the main chain is the interferometer optic. Three stages of blade (cantilever) springs provide vertical isolation. Sensor actuator devices (OSEMs) provide active damping and control in conjunction with an electrostatic drive (ESD). The reaction chain is used as a seismically isolated actuation surface.

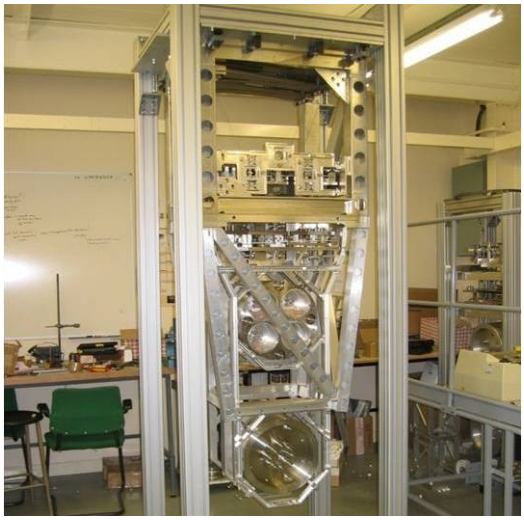

Fig. 5. Photograph of a prototype quadruple pendulum at Rutherford Appleton Lab in the UK. The two lower masses here are stainless steel dummy masses whereas in the production version they are fused silica glass. The two upper masses are almost entirely covered by the surrounding cage. The cage's purpose is to mount sensors, actuators, and to catch the masses. Copyright Science and Technology Facilities Council.

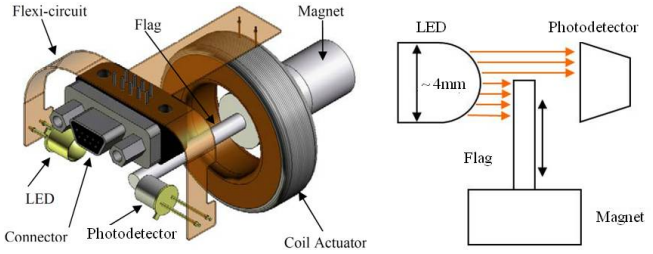

Fig. 6. A drawing of the working parts of an optical sensor electromagnet (OSEM). The OSEM consists of an LED, photodiode, and coil of wire. A flag mounted to a mass on the quadruple pendulum blocks part of the LED light and produces a position dependent signal from the photodiode. When a current is run through the coil an actuation force is produced on a permanent magnet mounted under the flag. Adapted from [8], [12].

electronic noise from the digital-to-analog converter (DAC) in the sensitive region of the LIGO interferometer at 10 Hz and above [9] (see Fig. 7). The current driver receives an input signal between $\pm 10\,\mathrm{V}$ from the DAC, allowing the actuator to apply a maximum of $0.205\,\mathrm{N}$ at zero frequency.

The OSEMs on the second mass from the top are the same model as those on the top and use the same magnets. However, the coil current driver has a different response due to the stricter noise requirements of being closer to the mirror. The DC gain is about 70 times lower than the top mass driver and the filter has a steeper roll off [10] (see Fig. 8). The maximum DC output of these OSEMs is $3.4\,\mathrm{mN}$.

At one stage away from the mirror the OSEMs on the third mass have an even more strict noise requirement, which is largely limited by the influence of stray environmental magnetic fields. Consequently, these OSEMs are a different model, with a much smaller magnet. They have a $5.25\,\mathrm{mm}$, 400 turn coil of wire, and actuate on a $6\,\mathrm{mm}$ long, $2\,\mathrm{mm}$ diameter magnet. The smaller coil and magnet pair makes these actuators much weaker than those on the higher stages, putting out only $16\,\mathrm{mN/A}$, at the benefit of much lower noise. Since the actuator is so weak, the filter in the current driver for the third mass does not need to be as steep as those for the second. See Fig. 9. These OSEMs can put out a maximum DC force of $43\,\mu\mathrm{N}$ [11].

B. Electrostatic Drive (ESD)

The most strict noise requirements are placed on the actuator at the mirror itself. Consequently, no magnets are permitted in order to avoid coupling with stray environmental magnetic fields. Physical contact of actuator parts with the mirror also increases mechanical loss and therefore creates suboptimal thermally excited fluctuations. These issues motivate the decision to use the ESD to actuate the mirror.

The ESD is described in detail in [13]. Fig. 10 shows a photograph of the reaction chain bottom mass highlighting the ESD. It has four quadrants, each with a pair of interlaced conductive gold traces. When a voltage difference is applied between these electrode pairs in each quadrant, the resulting electric field attracts the nearby parallel dielectric surface of the glass mirror in front of it.

The force each quadrant produces is nonlinear, given by

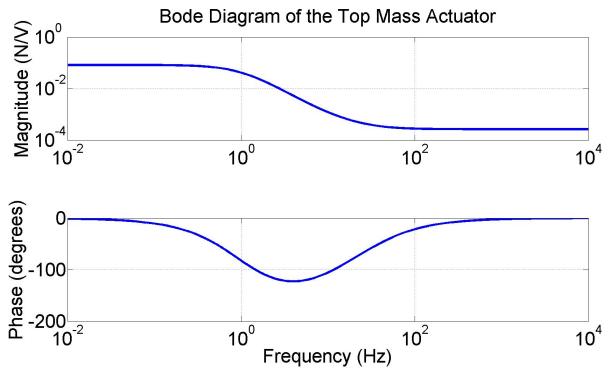

Fig. 7. The modeled transfer function in units of Newtons/Volt for the top stage actuation including the current driver and two coil-magnet pairs. The current driver has two poles at 1 Hz, and zeros at 10 Hz and 31 Hz [9].

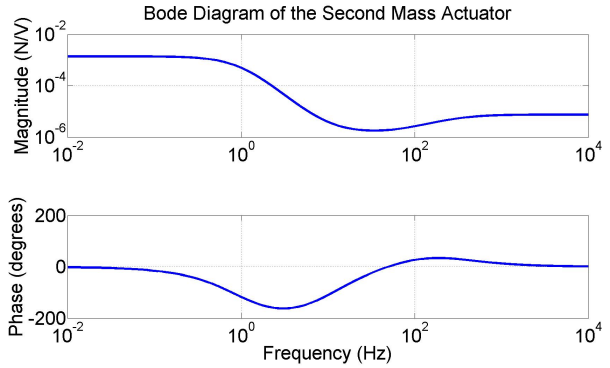

Fig. 8. The modeled transfer function in units of Newtons/Volt for the second stage actuation including the current driver and four coil-magnet pairs. The current driver has three poles at 1 Hz, one pole at 325 Hz, three zeros at 10 Hz, and one zero at 60 Hz [10].

$$F = \alpha(\Delta V)^2 = \alpha(V_{signal} - V_{bias})^2. \quad (1)$$

It is related by the square of the voltage difference between the two gold traces where a static bias voltage is applied to one and the control signal voltage is applied to the other. The coefficient α, known as the coupling coefficient is dependent not just on the geometry of the gold pattern but also on the gap size between the bottom stages of the two chains.

To use linear control analysis (1) is digitally linearized by setting V_{signal} to be V_{bias} plus the square root of the desired actuation. The dependence of α on the gap size cannot be removed, however, since the gap is not measured in this system. Nonetheless, the gap size may be considered constant since the relative motion between the mirror and ESD is small compared to the gap size, on the order of $10^{-7}\,\mathrm{m_{RMS}}$.

The speed of the actuator's response, many kHz, is much greater than the bandwidth of any reasonable design of an active control loop. Accordingly, (1) includes no delays.

The maximum ΔV for this ESD is 800V and the α is $2.9 \times 10^{-10}\,\mathrm{NV^{-2}}$. The values provide a maximum applied force of $190\,\mu$N. However, since the applied force is always attractive, bipolar actuation is achieved by implementing a static force offset set to half the maximum. This necessary offset limits our effective actuation to $95\,\mu$N.

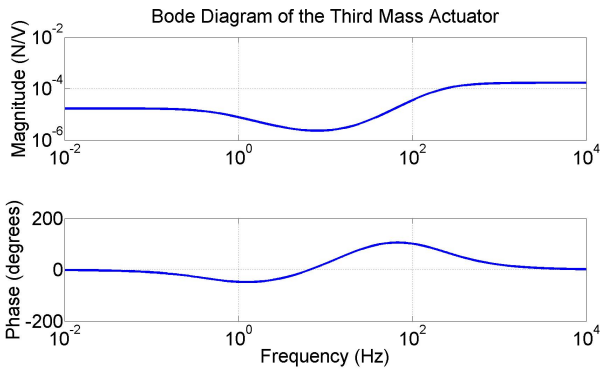

Fig. 9. The modeled transfer function in units of Newtons/Volt for the third stage actuation including the current driver and four coil-magnet pairs. The current driver has poles at 0.5 Hz, two at 200 Hz and zeros at 5 Hz and two at 20 Hz [11].

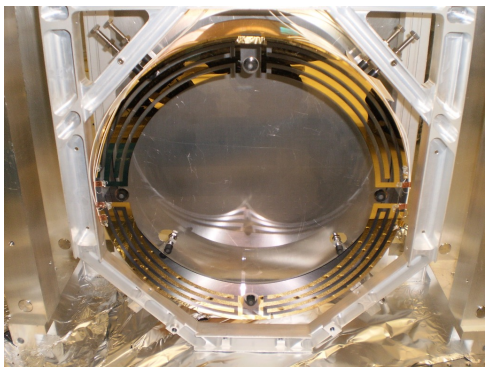

Fig. 10. A photograph of the quadruple pendulum prototype electrostatic drive (ESD) on the reaction chain bottom mass. Each quadrant has two interlaced gold traces. A potential difference between the traces will apply a force on the dielectric surface of the mirror 5 mm away.

V. Quadruple Pendulum Actuator Sizing

This section applies the pseudoinverse of the plant transfer function matrix to validate that the actuators provide sufficient dynamic range to fully reject the stochastic disturbances. This method is independent of feedback design, but does suggest characteristics of the optimal design.

The model of the pendulum used in this analysis is discussed in detail in [14], [15], [16] and has been verified against measured data. A reduced order version of the state space matrices is listed in the Appendix. The model was reduced by considering only motion of the stages of the pendulum along the axis of the beam path. The reduction is possible because the symmetry of the pendulum sufficiently decouples motion along this axis from all the others.

As discussed in Section II, the 'Advanced LIGO Total Noise' curve in Fig. 3 must be suppressed by pushing on the ETMs to maintain the interferometer at its optimal operating point. In other words, the control problem becomes a tracking one since the mirrors are actuated to follow as closely as possible this reference.

The block diagram in Fig. 11 summarizes the signal flow. In reality both ETMs are actuated on, but since they are conceptually identical, this loop is simplified by assuming there is only one. The position of the mirror, i.e. the bottom

mass of the pendulum, is measured interferometrically. This signal is compared to the desired position to generate the error signal. This error signal is passed to feedback filters that drive each of the four masses of the pendulum along the axis of the interferometer.

The frequency response of the sensors is ignored in this case to focus on the actuators. The DAC saturates at $\pm 10\,\mathrm{V}$, so the actuators must have enough dynamic range to maintain the DAC voltages, $\mathbf{u}$, within this limit.

To model the least mean square DAC voltages required to follow the desired trajectory R, the models of the actuators given in Section IV (plotted in Figs. 7, 8, and 9) are merged with the pendulum model in the Appendix to create a 1×4 plant $\mathbf{G}$. The goal of the control loop is to apply control forces to solve the transfer function (2). We assume the feedback loops have enough gain to approximate this simplification within the band of interest (up to $10\,\mathrm{kHz}$).

$$R = \mathbf{G}\mathbf{u} \tag{2}$$

R is taken to be the 'Advanced LIGO Total Noise' amplitude spectrum from Fig. 3 extended down to zero frequency (see Fig. 12).

The least squares DAC voltages, $\mathbf{u}_{ls}$, is given by the 4×1 pseudoinverse, $\mathbf{G}^{+}$.

However, since R is a random Gaussian signal given by the amplitude spectrum in Fig. 12, we do not need the phase information from $\mathbf{G}^{+}$. The amplitude spectrum of the least squares actuation $\mathbf{u}_{ls}$ is

$$\mathbf{u}_{ls} = |\mathbf{G}^{+}|R \tag{3}$$

where $|\mathbf{G}^{+}|$ is the real column vector containing the magnitudes of each complex element in $\mathbf{G}^{+}$.

Fig. 13 shows the resulting amplitude spectra of the DAC voltage sent to each actuator. The relative distance between values at each frequency represents the relative importance of each actuator. Larger values state higher importance. We see then that it is most advantageous to use the mirror actuator above $4\,\mathrm{Hz}$ while using the top mass actuator below. From a least squares point of view the second and third stage actuators gives us little.

Note that $\mathbf{G}^{+}$ (in general non-causal) does not represent a feedback control law, but rather the mapping of R to the minimum open loop force that would be required to move the mirror from rest to a trajectory with the amplitude spectrum of R. Thus, this least squares result sets a lower limit on an optimal feedback control design.

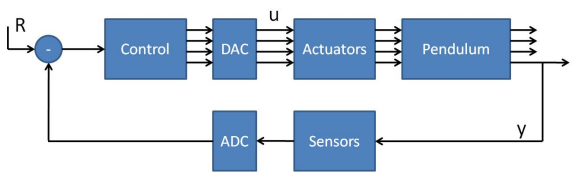

Fig. 11. The block diagram of the mirror positioning control loop. Actuation is applied on all four stages of the pendulum to control the position of the mirror, y, along the interferometer axis. The signals $\mathbf{u}$ must be maintained within the $\pm 10\,\mathrm{V}$ limit of the DAC.

The least squares RMS voltage for each actuator is found by integrating its power spectrum and taking the square root (Fig. 13). The probability of saturating the DAC at a given time step is calculated from the error function erf as,

$$p_i = 1 - \mathrm{erf}\left(\frac{10}{\sqrt{2}u_{i,RMS}}\right) \tag{4}$$

where p represents the probability of saturation at a given time step, i a particular actuator, u_{RMS} the RMS DAC voltage, and 10 is a scaling factor from the DAC saturation limit.

Table I summarizes the RMS DAC voltage and probability of saturation for the solution of the least squares actuation required at each stage. The top three actuators have virtually no risk of saturation. The mirror actuator comes the closest to saturation. If the spectrum of R is stationary then the mirror actuation also has practically no level of saturation.

However, on a stormy day R will increase and the control loops will demand more drive, possibly causing saturation at the mirror. Fortunately, the information in the table and in Fig. 13 provide hints as to how we might tune the control loops by telling us which actuators are most advantageous at which frequencies. This knowledge allows the actuation to be efficiently offloaded to other masses. Further, the finite bandwidth of the control loops, around $100\,\mathrm{Hz}$, reduces the force estimate needed at the mirror. The analysis in this paper assumes a feedback loop with broadband infinite gain, while we only need enough to limit the mirror motion to $10^{-15}\mathrm{m_{RMS}}$.

Additionally, we expect stormy weather to impact the low frequency band below $0.2\,\mathrm{Hz}$. It turns out that scaling the reference signal R in this band scales the voltages of the upper three stages given by Table I by a similar amount. The mirror voltage is largely unaffected. Thus, we can use these analysis techniques to conclude that from a least squares point of view we can tolerate an increase in R from stormy weather by a factor of 100, a reasonable margin.

Further, as indicated by Figure 13, the second and third stage actuators are doing very little here. Consequently, part of the mirror actuation can be offloaded to these stages to reduce the load at other stages at the expense of an increase in the total amount of drive. In fact, there are a number of other benefits for offloading the drive to higher stages. Perhaps the most important reason is stability. Crossing the top and bot-

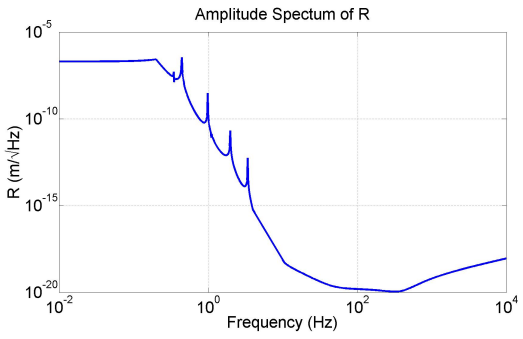

Fig. 12. Amplitude spectrum of the random Gaussian reference signal.

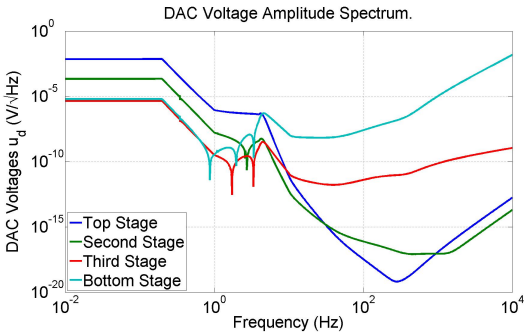

Fig. 13. Amplitude spectrum of the DAC voltages $\mathbf{u}_{ls}$.

TABLE I

THE LEAST SQUARES DAC VOLTAGES OF EACH ACTUATOR AND THE PROBABILITY p OF SATURATING AT THE ± 10 V LIMIT.

	RMS (V)	p
Top Stage	3.3×10^{-3}	0
Second Stage	1.0×10^{-4}	0
Third Stage	2.1×10^{-6}	0
Mirror	0.57	3.1×10^{-69}

tom stage actuation as steeply as the 4 Hz crossover shown in Fig. 13 will undoubtedly lead to a seriously unstable phase margin. Bridging the actuation bands at these two stages with even a small amount of drive at the stages in between will greatly improve the phase margin. Another powerful reason to offload control from the mirror is to minimize the impact of process noise injected through the actuators. Injecting noise at higher stages offers greater mechanical attenuation through the stages below.

VI. Conclusion

Using the pseudoinverse of the plant transfer function and the modeled system noise we have shown that the minimum mean square actuation required for the Advanced LIGO quadruple pendulum falls within the design constraints with reasonable margins. This analysis is possible without feedback loop design. Further, the pseudoinverse quantifies which actuator is most effective at each frequency providing critical information for later feedback design.

In general, additional analysis is needed during the design of any feedback loop since stability requirements will prevent the minimum mean square actuation from actually being achieved. The need to maintain reasonable phase margin prevents any given feedback filter from rolling off in magnitude too steeply. This limitation causes any error signal or noise outside the bandwidth of a particular actuator's loop to leak through and contribute to the RMS drive of that actuator.

VII. Acknowledgment

This work was supported by funding from the National Science Foundation under cooperative agreement PHY-0107417.

Appendix

The quadruple pendulum state space equations are listed here. $\mathbf{0}$ represents a zero matrix and $\mathbf{I}$ represents the identity matrix.

$$\dot{\mathbf{x}} = \mathbf{A}\mathbf{x} + \mathbf{B}\mathbf{u}, \quad y = \mathbf{C}\mathbf{x} + \mathbf{D}\mathbf{u} \tag{5}$$

$$\mathbf{x} = \begin{bmatrix} x_1 & x_2 & x_3 & x_4 & x_5 & x_6 & x_7 & x_8 \end{bmatrix}^T \tag{6}$$

$$\mathbf{u} = \begin{bmatrix} u_1 & u_2 & u_3 & u_4 \end{bmatrix}^T \tag{7}$$

$$\mathbf{A} = \left[\begin{array}{cccc:c} \multicolumn{4}{c:}{\mathbf{0}_{4\times4}} & \mathbf{0}_{4\times4} \\ \hdashline -297.3 & 163.5 & 0 & 0 & \\ 162.9 & -267.2 & 104.2 & 0 & -0.01\mathbf{I}_{4\times4} \\ 0 & 57.8 & -74.2 & 16.4 & \\ 0 & 0 & 16.4 & -16.4 & \end{array}\right] \tag{8}$$

$$\mathbf{B} = \left[\begin{array}{cccc} \multicolumn{4}{c}{\mathbf{0}_{4\times4}} \\ \hdashline 0.046 & 0 & 0 & 0 \\ 0 & 0.045 & 0 & 0 \\ 0 & 0 & 0.025 & 0 \\ 0 & 0 & 0 & 0.25 \end{array}\right] \tag{9}$$

$$\mathbf{C} = \left[\begin{array}{cccc:c} 0 & 0 & 0 & 1 & \mathbf{0}_{1\times4} \end{array}\right], \quad \mathbf{D} = \mathbf{0}_{1\times4} \tag{10}$$

References

[1] A. Abramovici, W. E. Althouse, R. W. P. Drever, Y. Gursel, S. Kawamura, F. J. Raab, D. Shoemaker, L. Sievers, R. E. Spero, and K. S. Thorne, "LIGO - The Laser Interferometer Gravitational-Wave Observatory," *Science*, vol. 256, pp. 325–333, Apr. 1992.

[2] B. C. Barish and R. Weiss, "LIGO and the detection of gravitational waves." *Physics Today*, vol. 52, pp. 44–50, Oct. 1999.

[3] J. Hough, S. Rowan, and B. S. Sathyaprakash, "The search for gravitational waves," *Journal of Physics B Atomic Molecular Physics*, vol. 38, pp. 497–+, May 2005.

[4] G. M. Harry and the LIGO Scientific Collaboration, "Advanced LIGO: the next generation of gravitational wave detectors," *Classical and Quantum Gravity*, vol. 27, no. 8, pp. 084 006–+, Apr. 2010.

[5] N. A. Robertson, G. Cagnoli, D. R. M. Crooks, E. Elliffe, J. E. Faller, P. Fritschel, S. Goßler, A. Grant, A. Heptonstall, J. Hough, H. Lück, R. Mittleman, M. Perreur-Lloyd, M. V. Plissi, S. Rowan, D. H. Shoemaker, P. H. Sneddon, K. A. Strain, C. I. Torrie, H. Ward, and P. Willems, "Quadruple suspension design for Advanced LIGO," *Classical and Quantum Gravity*, vol. 19, pp. 4043–4058, Aug. 2002.

[6] K. Thorne, *In 300 Years of Gravitation*. Cambridge University Press, Cambridge, 1987.

[7] D. Shoemaker, "Advanced LIGO Reference Design," LIGO, Internal Technical Document M060056, Mar. 2009.

[8] S. Aston and D. Hoyland, "Noise Prototype OSEM Design Document and Test Report," LIGO, Internal Technical Document T050111-02-K, Jan. 2008.

[9] J. Heefner, "UK Top Driver Pre-Production Prototype Test Plan," LIGO, Internal Technical Document T080014-v2, Apr. 2009.

[10] ——, "UK UIM Driver Pre-Production Prototype Test Plan," LIGO, Internal Technical Document T080021-v2, Dec. 2008.

[11] ——, "UK PUM Driver Pre-Production Prototype Test Plan," LIGO, Internal Technical Document T090164-v1, Apr. 2009.

[12] L. Ruet, "Active Control and Sensor Noise Filtering Duality Application to Advanced LIGO Suspensions," Ph.D. dissertation, Institut National des Sciences Appliques de Lyon (INSA Lyon), Jan. 2007.

[13] J. Miller, "On Non-Gaussian Beams and Optomechanical Parametric Instabilities in Interferometric Gravitational Wave Detectors," Ph.D. dissertation, University of Glasgow, Feb. 2010.

[14] M. Barton, "Models of the Advanced LIGO Suspensions in Mathematica^{TM}," LIGO, Internal Technical Document T020205-02D, June 2006.

[15] B. Shapiro, "Modal Control with State Estimation for Advanced LIGO Quadruple Suspensions," Master's thesis, Massachusetts Institute of Technology, Sept. 2007.

[16] B. Shapiro, "Fitting the Quad Noise Prototype Model to Measured Data," LIGO, Internal Technical Document T1000458, Aug. 2010.